Vector Fourier Analysis on Triangular Grids for Planar Elasticity

C. Rodrigo*

Abstract

In this paper Local Fourier Analysis (LFA) for multigrid methods on triangular grids is extended to the case of systems of PDEs. In particular, it is performed for the problem of planar elasticity, although its application to other systems is straightforward. Analogously to the scalar case, this analysis is based on an expression of the Fourier transform in new coordinate systems, both in space and in frequency variables, associated with reciprocal bases. LFA is particularly valuable for systems of PDEs, since it is often much more difficult to identify the correct multigrid components than for a scalar problem. For the discrete elasticity operator obtained with linear finite elements, different collective smoothers like three-color smoother and some zebra-type smoothers are analyzed. LFA results for these smoothers are presented.

1 Introduction

Planar elasticity models the displacements of an elastic body $\Omega \subset \mathbb{R}^2$, subject to a force density $\mathbf{f}$, with respect to its original configuration. These displacements are described by means of a vector function $\mathbf{u} = (u, v)$, which is the solution of the following system of equations

$$\mathbf{L}\,\mathbf{u} = -\mu\boldsymbol{\Delta}\mathbf{u} - (\lambda+\mu)\mathrm{grad}(\mathrm{div}\,\mathbf{u}) = \mathbf{f}, \quad \text{in } \Omega,$$

where $\boldsymbol{\Delta}$ is the vector Laplace operator, λ and μ are the so-called Lamè's coefficients, and $\mathbf{f} = (f_1, f_2) \in (L^2(\Omega))^2$. Here, a discretization by linear finite elements of this elasticity operator is considered,

$$\mathbf{L}_h = \begin{pmatrix} L_h^{u,u} & L_h^{u,v} \\ L_h^{v,u} & L_h^{v,v} \end{pmatrix} = \begin{pmatrix} -(\lambda+2\mu)(\partial_{xx})_h - \mu(\partial_{yy})_h & -(\lambda+\mu)(\partial_{xy})_h \\ -(\lambda+\mu)(\partial_{xy})_h & -\mu(\partial_{xx})_h - (\lambda+2\mu)(\partial_{yy})_h \end{pmatrix}.$$

The algebraic linear equation system arising from this discretization will be solved by means of a geometric multigrid algorithm, due to the fact that these methods are among the most efficient numerical algorithms for solving this kind of systems. In geometric multigrid, a hierarchy of grids must be proposed. For an irregular domain, it is very common to apply regular refinement to an unstructured input grid; in this way, a hierarchy of globally unstructured grids is generated that is suitable for use with geometric multigrid. So, we are interested in the framework of hierarchical hybrid grids (HHG) which was presented in [1]. The coarsest mesh is assumed rough enough in order to fit the geometry of the domain. Once this coarse triangulation is given, each triangle is divided into four congruent triangles connecting the midpoints of their edges, and so forth until the mesh has the desired fine scale to approximate the solution of the problem. In this way, a nested hierarchy of grids is obtained.

As it is well-known, the construction of an efficient multigrid method is strongly dependent on the choice of its components, which have to be selected so that they efficiently interplay with each other. Especially, the choice of a suitable smoother is an important feature for the design of an efficient multigrid method. In this paper, a linear interpolation has been chosen, the restriction operator has been taken as its adjoint and the discrete operator corresponding to each mesh results from the direct

*Department of Applied Mathematics, University of Zaragoza, Spain. E-mail: carmenr@unizar.es

discretization of the problem. Moreover, collective three-color smoother and some collective line-wise smoothers of zebra-type are proposed as relaxing methods.

In order to choose suitable components for a multigrid method, LFA is used, due to its being a powerful tool for the design of efficient multigrid methods. This analysis is mainly based on the Fourier transform and was introduced by Brandt [2]. A good introduction can be found in the books by Trottenberg et al. [4] and Wienands and Joppich [5]. This technique has been widely used in the framework of discretizations on rectangular grids, and recently a generalization to triangular grids has been proposed in [3]. The key fact for carrying out this generalization is to write the Fourier transform using coordinates in non-orthogonal bases fitting the new structure of the grid. In order to extend LFA to the case of the planar elasticity system, a new expression of the Fourier transform for vector functions is considered. To study multigrid methods in the framework of HHG, the LFA proposed here is applied to each input triangle in such a way that the global behavior of the method will depend on the quality of the chosen local components.

The organization of the paper is as follows. In Section 2, the way in which LFA is performed, particularly for the case of the considered smoothers, is explained. In Section 2.1, the new expression of the Fourier transform is presented and some concepts necessary for the development of LFA are introduced. Section 2.2 explains the performance of LFA smoothing analysis for three-color and zebra-type smoothers, and two-grid analysis is described in Section 2.3. Finally, in Section 3, some LFA results are presented in order to choose the components of the multigrid algorithm which are more suitable for different grid geometries.

2 Fourier analysis

2.1 General definitions

A non-orthogonal unitary basis of $\mathbb{R}^2$ is established: $\{\mathbf{e}_1', \mathbf{e}_2'\}$ with $0 < \gamma < \pi$ being the angle between the vectors of the basis. It is also considered its reciprocal basis $\{\mathbf{e}_1'', \mathbf{e}_2''\}$, i.e., $(\mathbf{e}_i', \mathbf{e}_j'') = \delta_{ij}$, $1 \leq i, j \leq 2$, where $(\cdot, \cdot)$ is the usual inner product in $\mathbb{R}^2$ and δ_{ij} is the Kronecker's delta, see Figure 1. The coordinates of a point in these bases, $\{\mathbf{e}_1', \mathbf{e}_2'\}$ and $\{\mathbf{e}_1'', \mathbf{e}_2''\}$, are $\mathbf{y}' = (y_1', y_2')$ and $\mathbf{y}'' = (y_1'', y_2'')$, respectively, just like $\mathbf{y} = (y_1, y_2)$ in the canonical basis $\{\mathbf{e}_1, \mathbf{e}_2\}$.

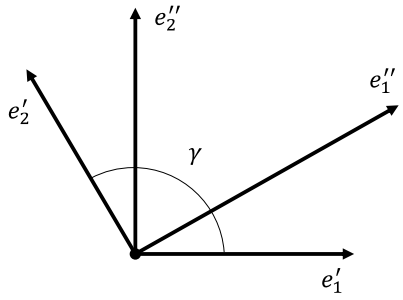

Figure 1: Reciprocal bases in $\mathbb{R}^2$.

By applying the changes of variables $\mathbf{x} = \mathbf{F}(\mathbf{x}')$ and $\boldsymbol{\theta} = \mathbf{G}(\boldsymbol{\theta}'')$ to the usual Fourier transform formula, the Fourier transform and its corresponding back transformation formula with coordinates in a non-orthogonal basis, result in the following

$$\hat{\mathbf{u}}(\mathbf{G}(\boldsymbol{\theta}'')) = \frac{\sin\gamma}{2\pi} \int_{\mathbb{R}^2} e^{-i\mathbf{G}(\boldsymbol{\theta}'')\cdot\mathbf{F}(\mathbf{x}')} \mathbf{u}(\mathbf{F}(\mathbf{x}'))\, \mathrm{d}\mathbf{x}', \quad \mathbf{u}(\mathbf{F}(\mathbf{x}')) = \frac{1}{2\pi \sin\gamma} \int_{\mathbb{R}^2} e^{i\mathbf{G}(\boldsymbol{\theta}'')\cdot\mathbf{F}(\mathbf{x}')} \hat{\mathbf{u}}(\mathbf{G}(\boldsymbol{\theta}''))\, \mathrm{d}\boldsymbol{\theta}''.$$

Since the new bases are reciprocal bases, the inner product $\mathbf{G}(\boldsymbol{\theta}'')\cdot\mathbf{F}(\mathbf{x}')$ is given by $\theta_1''x_1'+\theta_2''x_2'$. Using previous expressions, a discrete Fourier transform for non-rectangular grids can be introduced. With this purpose, a uniform infinite grid $G_h=\{\mathbf{x}'=(x_1',x_2')\,|\,x_i'=k_ih_i,\ k_i\in\mathbb{Z},\ i=1,2\}$, is defined, where $\mathbf{h}=(h_1,h_2)$ is a grid spacing. Now, for a vector grid function $\mathbf{u}_h$, the discrete Fourier transform and its back Fourier transformation can be defined by

$$\hat{\mathbf{u}}_h(\boldsymbol{\theta}'')=\frac{h_1h_2\sin\gamma}{2\pi}\sum_{\mathbf{x}'\in G_h}e^{-i(\theta_1''x_1'+\theta_2''x_2')}\mathbf{u}_h(\mathbf{x}'),\quad \mathbf{u}_h(\mathbf{x}')=\frac{1}{2\pi\sin\gamma}\int_{\boldsymbol{\Theta}_h}e^{i(\theta_1''x_1'+\theta_2''x_2')}\hat{\mathbf{u}}_h(\boldsymbol{\theta}'')\mathrm{d}\boldsymbol{\theta}'',\quad (1)$$

where $\boldsymbol{\theta}''=(\theta_1'',\theta_2'')\in\boldsymbol{\Theta}_h=(-\pi/h_1,\pi/h_1]\times(-\pi/h_2,\pi/h_2]$ are the coordinates of the point $\theta_1''\mathbf{e}_1''+\theta_2''\mathbf{e}_2''$ in the frequency space. Considering the scalar Fourier modes, $\varphi_h(\boldsymbol{\theta}'',\mathbf{x}')=\mathrm{e}^{i\theta_1''x_1'}\,\mathrm{e}^{i\theta_2''x_2'}$, their vector counterparts are $\boldsymbol{\varphi}_h(\boldsymbol{\theta}'',\mathbf{x}'):=\big(\varphi_h(\boldsymbol{\theta}'',\mathbf{x}'),\varphi_h(\boldsymbol{\theta}'',\mathbf{x}')\big)^t$, with $\mathbf{x}'\in G_h$, and $\boldsymbol{\theta}''\in\boldsymbol{\Theta}_h$. They give rise to the Fourier space, $\mathcal{F}(G_h)=\mathrm{span}\{\boldsymbol{\varphi}_h(\boldsymbol{\theta}'',\cdot)\,|\,\boldsymbol{\theta}''\in\boldsymbol{\Theta}_h\}$. From (1), it follows that each discrete function $\mathbf{u}_h(\mathbf{x}')\in(l_h^2(G_h))^2$ can be written as a formal linear combination of the Fourier modes, which are linearly independent discrete functions.

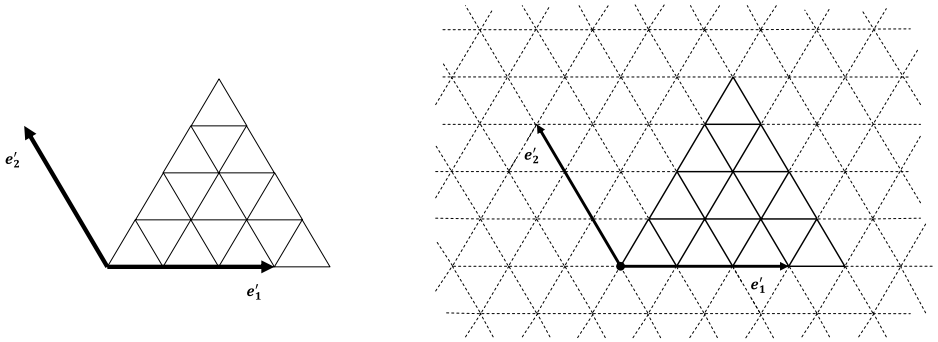

Figure 2: Regular triangular grid on a fixed coarse triangle $\mathcal{T}$ and its extension to an infinite grid.

Let $\mathcal{T}_h$ be a regular triangular grid on a fixed coarse triangle $\mathcal{T}$; see left picture of Figure 2. $\mathcal{T}_h$ is extended to the infinite grid G_h given before, where $\mathbf{e}_1'$ and $\mathbf{e}_2'$ are unit vectors indicating the direction of two of the edges of $\mathcal{T}$, and such that $\mathcal{T}_h=G_h\bigcap\mathcal{T}$, see right picture of Figure 2. Neglecting boundary conditions and/or connections with other neighboring triangles of the coarsest grid, the discrete problem $\mathbf{L}_h\mathbf{u}_h=\mathbf{f}_h$ can be extended to the whole grid G_h. As it is well-known, vector Fourier modes $\boldsymbol{\varphi}_h(\boldsymbol{\theta}'',\mathbf{x}')$ are formal eigenfunctions of the discrete operator $\mathbf{L}_h$. More precisely, it is fulfilled

$$\mathbf{L}_h\boldsymbol{\varphi}_h(\boldsymbol{\theta}'',\mathbf{x}')=\widetilde{\mathbf{L}}_h(\boldsymbol{\theta}'')\boldsymbol{\varphi}_h(\boldsymbol{\theta}'',\mathbf{x}')=\begin{pmatrix}\widetilde{L}_h^{u,u}(\boldsymbol{\theta}'') & \widetilde{L}_h^{u,v}(\boldsymbol{\theta}'')\\ \widetilde{L}_h^{v,u}(\boldsymbol{\theta}'') & \widetilde{L}_h^{v,v}(\boldsymbol{\theta}'')\end{pmatrix}\boldsymbol{\varphi}_h(\boldsymbol{\theta}'',\mathbf{x}'),$$

where matrix $\widetilde{\mathbf{L}}_h(\boldsymbol{\theta}'')$ is the Fourier symbol of $\mathbf{L}_h$.
Using standard coarsening, high and low frequency components on G_h are distinguished, in the way that the subset of low frequencies is $\boldsymbol{\Theta}_{2h}=(-\pi/2h_1,\pi/2h_1]\times(-\pi/2h_2,\pi/2h_2]$, and the subset of high frequencies is $\boldsymbol{\Theta}_h\setminus\boldsymbol{\Theta}_{2h}$.
For simplicity in notation, in the following we will use $\mathbf{x}=(x_1,x_2)$ and $\boldsymbol{\theta}=(\theta_1,\theta_2)$ as the coordinate vectors in the bases $\{\mathbf{e}_1',\mathbf{e}_2'\}$ and $\{\mathbf{e}_1'',\mathbf{e}_2''\}$, respectively.

2.2 Smoothing analysis

In Fourier smoothing analysis, the influence of a smoothing operator on the high-frequency error components is investigated. An ideal coarse grid operator which annihilates the low-frequency error components and leaves the high-frequency components unchanged is assumed. This paper focuses on the analysis of three-color smoother and different variants of zebra-type smoothers because, like other multicolor-type relaxations, their analysis is a bit different from that of standard smoothers, due to the fact that Fourier modes are no longer their eigenfunctions.

2.2.1 Smoothing analysis for three–color smoother

To apply three-color smoother, first the infinite grid must be split into three disjoint subgrids, each of them associated with a different color, as shown in Figure 3, so that the unknowns of the same color have no direct connection with each other,

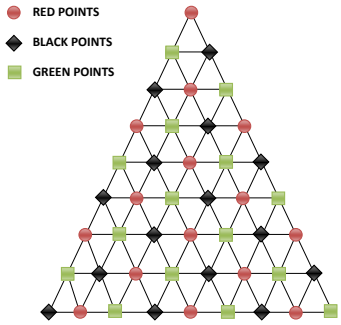

Figure 3: Three-color smoother.

$$G_h^i = \{\mathbf{x} = (x_1, x_2)\,|\,x_j = k_j h_j,\ k_j \in \mathbb{Z},\ j = 1,2,\ k_1 + k_2 = i\,(\mathrm{mod}\,3)\}, \quad i = 0,1,2.$$

The complete three-color smoothing operator is given by the product of three partial operators, $\mathbf{S}_h(\omega) = \mathbf{S}_h^2(\omega)\mathbf{S}_h^1(\omega)\mathbf{S}_h^0(\omega)$. In each partial relaxation step, only the grid points of G_h^i are processed, whereas the remaining points are not treated, that is,

$$\mathbf{S}_h^i(\omega)\mathbf{v}_h(\mathbf{x}) = \begin{cases} [(\mathbf{I}_h - \omega\mathbf{D}_h^{-1}\mathbf{L}_h)\mathbf{v}_h](\mathbf{x}), & \mathbf{x} \in G_h^i, \\ \mathbf{v}_h(\mathbf{x}), & \mathbf{x} \in G_h \backslash G_h^i, \end{cases}$$

where $\mathbf{D}_h$ is the diagonal part of the discrete operator $\mathbf{L}_h$, $\mathbf{I}_h$ is the identity operator and ω is a relaxation parameter.
This smoother couples certain Fourier modes and therefore, we consider an appropriate decomposition of the Fourier space given by

$$\mathcal{F}(G_h) = \oplus\mathcal{F}^3(\boldsymbol{\theta}_{00}), \qquad \mathcal{F}^3(\boldsymbol{\theta}_{00}) = \mathrm{span}\{\boldsymbol{\varphi}_h(\boldsymbol{\theta}_{00},\cdot), \boldsymbol{\varphi}_h(\boldsymbol{\theta}_{11},\cdot), \boldsymbol{\varphi}_h(\boldsymbol{\theta}_{22},\cdot)\}, \tag{2}$$

where $\boldsymbol{\theta}_{\alpha\alpha} = (\boldsymbol{\theta}_{00} - \frac{2\pi\alpha}{3}\mathbf{h}^{-1})(\mathrm{mod}\,2\pi\mathbf{h}^{-1})$, $\alpha = 0,1,2$, $\mathbf{h}^{-1} = (h_1^{-1}, h_2^{-1})$ and Fourier frequencies $\boldsymbol{\theta}_{00}$ are taken into an L–shaped region as depicted in Figure 4

$$\boldsymbol{\theta}_{00} \in \boldsymbol{\Lambda}^3 = \left(\left(-\frac{\pi}{3h_1}, \frac{\pi}{h_1}\right] \times \left(-\frac{\pi}{3h_2}, \frac{\pi}{h_2}\right]\right) \setminus \left(\left(\frac{\pi}{3h_1}, \frac{\pi}{h_1}\right] \times \left(\frac{\pi}{3h_2}, \frac{\pi}{h_2}\right]\right).$$

With this decomposition, it is obtained that operators $\mathbf{S}_h^i(\omega)$ leave invariant the subspaces $\mathcal{F}^3(\boldsymbol{\theta}_{00})$. In particular, for operator $\mathbf{S}_h^0$, for example, the following equality is fulfilled,

$$\mathbf{S}_h^0(\omega)\begin{pmatrix} \boldsymbol{\varphi}_h(\boldsymbol{\theta}_{00},\cdot) \\ \boldsymbol{\varphi}_h(\boldsymbol{\theta}_{11},\cdot) \\ \boldsymbol{\varphi}_h(\boldsymbol{\theta}_{22},\cdot) \end{pmatrix} = \frac{1}{3}\begin{pmatrix} \mathbf{A}_{00}(\boldsymbol{\theta}_{00},\omega) & \mathbf{A}_{11}(\boldsymbol{\theta}_{00},\omega) & \mathbf{A}_{22}(\boldsymbol{\theta}_{00},\omega) \\ \mathbf{A}_{00}(\boldsymbol{\theta}_{11},\omega) & \mathbf{A}_{11}(\boldsymbol{\theta}_{11},\omega) & \mathbf{A}_{22}(\boldsymbol{\theta}_{11},\omega) \\ \mathbf{A}_{00}(\boldsymbol{\theta}_{22},\omega) & \mathbf{A}_{11}(\boldsymbol{\theta}_{22},\omega) & \mathbf{A}_{22}(\boldsymbol{\theta}_{22},\omega) \end{pmatrix}\begin{pmatrix} \boldsymbol{\varphi}_h(\boldsymbol{\theta}_{00},\cdot) \\ \boldsymbol{\varphi}_h(\boldsymbol{\theta}_{11},\cdot) \\ \boldsymbol{\varphi}_h(\boldsymbol{\theta}_{22},\cdot) \end{pmatrix}, \tag{3}$$

with

$$\mathbf{A}_{\alpha'\alpha'}(\boldsymbol{\theta}_{\alpha\alpha},\omega) = \begin{cases} \boldsymbol{\lambda}_{\alpha\alpha}(\omega) + 2\mathbf{I}, & \text{if } \alpha' = \alpha, \\ \boldsymbol{\lambda}_{\alpha\alpha}(\omega) - \mathbf{I}, & \text{otherwise,} \end{cases}$$

where $\mathbf{I}$ is the (2×2)-identity matrix and $\boldsymbol{\lambda}_{\alpha\alpha}(\omega)$ is the (2×2)–matrix $\boldsymbol{\lambda}_{\alpha\alpha}(\omega) = \widetilde{\mathbf{I}}_h - \omega\widetilde{\mathbf{D}}_h^{-1}(\boldsymbol{\theta}_{\alpha\alpha})\widetilde{\mathbf{L}}_h(\boldsymbol{\theta}_{\alpha\alpha})$. Formula (3) gives us the expression of the Fourier representation of the partial operator $\mathbf{S}_h^0$ in the subspace $\mathcal{F}^3(\boldsymbol{\theta}_{00})$, denoted by $\widehat{\mathbf{S}}_h^0(\boldsymbol{\theta}_{00},\omega)$. In an analogous way, it is possible to obtain the corresponding

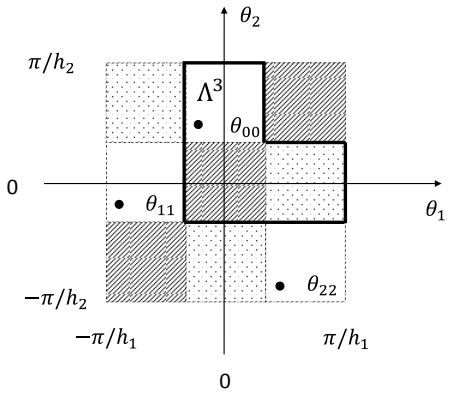

Figure 4: Three–dimensional minimal invariant harmonic subspaces for three–color smoother.

representations of $\mathbf{S}_h^1$ and $\mathbf{S}_h^2$, denoted by $\widehat{\mathbf{S}}_h^1(\boldsymbol{\theta}_{00},\omega)$ and $\widehat{\mathbf{S}}_h^2(\boldsymbol{\theta}_{00},\omega)$, respectively, which are composed of matrices $\mathbf{B}_{\alpha'\alpha'}(\boldsymbol{\theta}_{\alpha\alpha},\omega)$ and $\mathbf{C}_{\alpha'\alpha'}(\boldsymbol{\theta}_{\alpha\alpha},\omega)$ given in the following way

$$\mathbf{B}_{\alpha'\alpha'}(\boldsymbol{\theta}_{\alpha\alpha},\omega)=\begin{cases}\boldsymbol{\lambda}_{\alpha\alpha}(\omega)+2\mathbf{I}, & \text{if } \alpha'=\alpha,\\ e^{-2\pi i/3}\boldsymbol{\lambda}_{\alpha\alpha}(\omega)+(e^{2\pi i/3}+1)\mathbf{I}, & \text{if } \alpha'=\alpha+1 \pmod 3,\\ e^{2\pi i/3}\boldsymbol{\lambda}_{\alpha\alpha}(\omega)+(e^{-2\pi i/3}+1)\mathbf{I}, & \text{if } \alpha'=\alpha+2 \pmod 3,\end{cases}$$

$$\mathbf{C}_{\alpha'\alpha'}(\boldsymbol{\theta}_{\alpha\alpha},\omega)=\overline{\mathbf{B}_{\alpha'\alpha'}(\boldsymbol{\theta}_{\alpha\alpha},\omega)}.$$

The mean smoothing factor, for ν consecutive sweeps, is $\mu(\mathbf{S}_h(\omega),\nu)=\sup_{\boldsymbol{\theta}_{00}\in\boldsymbol{\Lambda}^3}\{\sqrt[\nu]{\rho(\widehat{\mathbf{Q}}(\boldsymbol{\theta}_{00})\widehat{\mathbf{S}}_h^{\nu}(\boldsymbol{\theta}_{00},\omega))}\}$, where $\widehat{\mathbf{Q}}(\boldsymbol{\theta}_{00})$ is a projection matrix, which annihilates the low–frequency error components and leaves the high–frequency ones unchanged, given by $\widehat{\mathbf{Q}}(\boldsymbol{\theta}_{00})=\mathrm{diag}\{\mathbf{P}(\boldsymbol{\theta}_{00}),\mathbf{P}(\boldsymbol{\theta}_{11}),\mathbf{P}(\boldsymbol{\theta}_{22})\}$, where $\mathbf{P}(\boldsymbol{\theta}_{\alpha\alpha})$ is the (2×2)–null matrix when $\boldsymbol{\theta}_{\alpha\alpha}\in\boldsymbol{\Theta}_{2h}$, and the (2×2)–identity matrix otherwise.

2.2.2 Smoothing analysis for zebra-type smoothers

Zebra-type smoothers consist of two half steps. In the first half-step, odd lines are processed, whereas even lines are relaxed in the second step, in which the updated approximations on the odd lines are used. For triangular grids, three different zebra smoothers can be defined on a triangle as shown in Figure 5. They will be denoted as zebra-red, zebra-black and zebra-green smoothers, since they correspond to each of the vertices of the triangle.

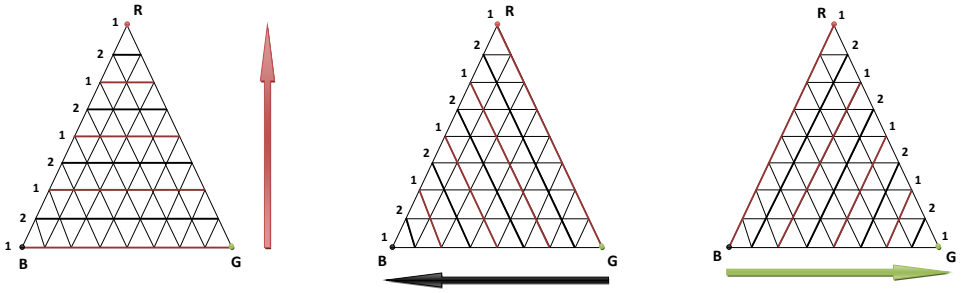

Figure 5: Zebra line smoothers: approximations at points marked by 1 are updated in the first half-step of the relaxation, those marked by 2 in the second.

In order to perform these smoothers, a splitting of the grid G_h into two different subsets G_h^{even} and G_h^{odd} is necessary. For each of the zebra smoothers these subgrids are defined in a different way, and the corresponding distinction between them is specified in Table 1. Thus, these three smoothers $\mathbf{S}_h^{zR}$,

Relaxation	G_h^{even}	G_h^{odd}
Zebra-red	k_2 even	k_2 odd
Zebra-black	k_1 even	k_1 odd
Zebra-green	$k_1 + k_2$ even	$k_1 + k_2$ odd

Table 1: Characterization of subgrids G_h^{even} and G_h^{odd} for different zebra smoothers.

$\mathbf{S}_h^{zB}$ and $\mathbf{S}_h^{zG}$ are defined by the product of two partial operators. For example, if zebra-red smoother is considered, $\mathbf{S}_h^{zR} = \mathbf{S}_h^{zR-even} \cdot \mathbf{S}_h^{zR-odd}$ where $\mathbf{S}_h^{zR-even}$ is in charge of relaxing the points in G_h^{even} and $\mathbf{S}_h^{zR-odd}$ is responsible for the points in G_h^{odd}. For this zebra-red smoother, it is fulfilled

$$\mathbf{S}_h^{zR-even}\,\boldsymbol{\varphi}_h(\boldsymbol{\theta},\mathbf{x}) = \begin{cases} \mathbf{A}(\boldsymbol{\theta})\,\boldsymbol{\varphi}_h(\boldsymbol{\theta},\mathbf{x}), & \mathbf{x} \in G_h^{even} \\ \boldsymbol{\varphi}_h(\boldsymbol{\theta},\mathbf{x}), & \mathbf{x} \in G_h^{odd} \end{cases}, \quad \mathbf{S}_h^{zR-odd}\,\boldsymbol{\varphi}_h(\boldsymbol{\theta},\mathbf{x}) = \begin{cases} \boldsymbol{\varphi}_h(\boldsymbol{\theta},\mathbf{x}), & \mathbf{x} \in G_h^{even} \\ \mathbf{A}(\boldsymbol{\theta})\,\boldsymbol{\varphi}_h(\boldsymbol{\theta},\mathbf{x}), & \mathbf{x} \in G_h^{odd} \end{cases},$$

where $\mathbf{A}(\boldsymbol{\theta})$ is a (2×2)-matrix.
These relaxation operators couple Fourier components, in particular they leave invariant certain low-dimensional subspaces of the Fourier space, which are two-dimensional ones. However, for the convenience of the two-grid analysis, the following four-dimensional subspaces, which are called spaces of $2h$-harmonics are considered, $\mathcal{F}^4(\boldsymbol{\theta}^{00}) = \text{span}\{\boldsymbol{\varphi}_h(\boldsymbol{\theta}^{00},\cdot), \boldsymbol{\varphi}_h(\boldsymbol{\theta}^{11},\cdot), \boldsymbol{\varphi}_h(\boldsymbol{\theta}^{10},\cdot), \boldsymbol{\varphi}_h(\boldsymbol{\theta}^{01},\cdot)\}$, with $\boldsymbol{\theta}^{00} = (\theta_1^{00}, \theta_2^{00}) \in \boldsymbol{\Theta}_{2h}$, and $\boldsymbol{\theta}^{11}$, $\boldsymbol{\theta}^{10}$ and $\boldsymbol{\theta}^{01}$ defined by

$$\boldsymbol{\theta}^{ij} = \boldsymbol{\theta}^{00} - (i\,\text{sign}(\theta_1^{00})\pi/h_1, j\,\text{sign}(\theta_2^{00})\pi/h_2),\ i,j \in \{0,1\}. \tag{4}$$

It is obvious that the $2h$-harmonics generate the whole Fourier space $\mathcal{F}(G_h) = \oplus\mathcal{F}^4(\boldsymbol{\theta}_{00})$, and thus, since these subspaces remain invariant under the application of zebra-type smoothers, a block Fourier representation of the smoothing operator which permits an easy calculation of smoothing factors can be obtained. Hence, Fourier representation of the operator based on the $2h$-harmonics reads

$$\widehat{\mathbf{S}}_h^{zR}(\boldsymbol{\theta}) = \widehat{\mathbf{S}}_h^{zR-even}(\boldsymbol{\theta}) \cdot \widehat{\mathbf{S}}_h^{zR-odd}(\boldsymbol{\theta}),$$

with

$$\widehat{\mathbf{S}}_h^{zR-even}(\boldsymbol{\theta}) = \frac{1}{2}\begin{pmatrix} \mathbf{A}(\boldsymbol{\theta}^{00}) + \mathbf{I} & \mathbf{0} & \mathbf{0} & \mathbf{A}(\boldsymbol{\theta}^{01}) - \mathbf{I} \\ \mathbf{0} & \mathbf{A}(\boldsymbol{\theta}^{11}) + \mathbf{I} & \mathbf{A}(\boldsymbol{\theta}^{10}) - \mathbf{I} & \mathbf{0} \\ \mathbf{0} & \mathbf{A}(\boldsymbol{\theta}^{11}) - \mathbf{I} & \mathbf{A}(\boldsymbol{\theta}^{10}) + \mathbf{I} & \mathbf{0} \\ \mathbf{A}(\boldsymbol{\theta}^{00}) - \mathbf{I} & \mathbf{0} & \mathbf{0} & \mathbf{A}(\boldsymbol{\theta}^{01}) + \mathbf{I} \end{pmatrix},$$

$$\widehat{\mathbf{S}}_h^{zR-odd}(\boldsymbol{\theta}) = \frac{1}{2}\begin{pmatrix} \mathbf{A}(\boldsymbol{\theta}^{00}) + \mathbf{I} & \mathbf{0} & \mathbf{0} & -\mathbf{A}(\boldsymbol{\theta}^{01}) + \mathbf{I} \\ \mathbf{0} & \mathbf{A}(\boldsymbol{\theta}^{11}) + \mathbf{I} & -\mathbf{A}(\boldsymbol{\theta}^{10}) + \mathbf{I} & \mathbf{0} \\ \mathbf{0} & -\mathbf{A}(\boldsymbol{\theta}^{11}) + \mathbf{I} & \mathbf{A}(\boldsymbol{\theta}^{10}) + \mathbf{I} & \mathbf{0} \\ -\mathbf{A}(\boldsymbol{\theta}^{00}) + \mathbf{I} & \mathbf{0} & \mathbf{0} & \mathbf{A}(\boldsymbol{\theta}^{01}) + \mathbf{I} \end{pmatrix},$$

where $\mathbf{0}$ is the (2×2)-null matrix, and $\boldsymbol{\theta} = \boldsymbol{\theta}^{00} \in \boldsymbol{\Theta}_{2h}$. Analogously, Fourier representations of the zebra-black and zebra-green smoothers can be obtained.

2.3 Two-grid analysis

In order to investigate the interplay between relaxation and coarse grid correction, which is crucial for an efficient multigrid method, it is convenient to perform a two-grid analysis which takes into account the effect of transfer operators. Let $\mathbf{u}_h^m$ be an approximation of $\mathbf{u}_h$. The error $\mathbf{e}^m = \mathbf{u}_h^m - \mathbf{u}_h$ is transformed by a two-grid cycle as $\mathbf{e}^{m+1} = \mathbf{M}_h^{2h}\mathbf{e}^m$, where $\mathbf{M}_h^{2h} = \mathbf{S}_h^{\nu_2}\mathbf{K}_h^{2h}\mathbf{S}_h^{\nu_1}$ is the two-grid operator, $\mathbf{K}_h^{2h} = (\mathbf{I}_h - \mathbf{P}_{2h}^h(\mathbf{L}_{2h})^{-1}\mathbf{R}_h^{2h}\mathbf{L}_h)$ the coarse grid correction operator and $\mathbf{S}_h$ is a smoothing operator on G_h with ν_1 and ν_2 indicating the number of pre– and post–smoothing steps respectively. In the

definition of $\mathbf{K}_h^{2h}$, $\mathbf{L}_{2h}$ is the coarse grid operator and $\mathbf{P}_{2h}^h$, $\mathbf{R}_h^{2h}$ are transfer operators from coarse to fine grids and vice versa. The two–grid analysis is the basis for the classical asymptotic multigrid convergence estimates, and the spectral radius $\rho(\mathbf{M}_h^{2h})$ of the operator $\mathbf{M}_h^{2h}$ indicates the convergence factor of the multigrid method.
In order to guarantee that nonsingular Fourier symbols $\widetilde{\mathbf{L}}_h(\boldsymbol{\theta})$ and $\widetilde{\mathbf{L}}_{2h}(2\boldsymbol{\theta})$ are taken, we restrict our considerations to $\tilde{\boldsymbol{\Theta}}_{2h} = \boldsymbol{\Theta}_{2h} \setminus \boldsymbol{\Psi}$, where

$$\boldsymbol{\Psi} = \{\boldsymbol{\theta}^{00} \in \boldsymbol{\Theta}_{2h} \mid \det(\widetilde{\mathbf{L}}_{2h}(2\boldsymbol{\theta}^{00})) = 0, \text{ or } \det(\widetilde{\mathbf{L}}_h(\boldsymbol{\theta}^{ij})) = 0,\ i,j \in \{0,1\}\}.$$

As it is well-known, the coarse grid correction operator $\mathbf{K}_h^{2h}$ leaves the four–dimensional subspace of $2h$–harmonics $\mathcal{F}^4(\boldsymbol{\theta}^{00})$ invariant for an arbitrary Fourier frequency $\boldsymbol{\theta}^{00} \in \tilde{\boldsymbol{\Theta}}_{2h}$. The same invariance property holds for many well–known smoothers, like zebra-type smoothers. Therefore, the two–grid operator $\mathbf{M}_h^{2h} = \mathbf{S}_h^{\nu_2}\mathbf{K}_h^{2h}\mathbf{S}_h^{\nu_1}$ also leaves the $2h$–harmonic subspaces invariant, and as a consequence it is equivalent to a block-diagonal matrix, consisting of (8×8)–blocks, denoted by

$$\widehat{\mathbf{M}}_h^{2h}(\boldsymbol{\theta}^{00}) = (\widehat{\mathbf{S}}_h(\boldsymbol{\theta}^{00}))^{\nu_2}\widehat{\mathbf{K}}_h^{2h}(\boldsymbol{\theta}^{00})(\widehat{\mathbf{S}}_h(\boldsymbol{\theta}^{00}))^{\nu_1},$$

with $\boldsymbol{\theta}^{00} \in \tilde{\boldsymbol{\Theta}}_{2h}$ and where the Fourier representation of the relaxation method is an (8×8)-matrix, $\widehat{\mathbf{S}}_h(\boldsymbol{\theta})$, and the block-matrix representation of the coarse grid correction in the subspace $\mathcal{F}^4(\boldsymbol{\theta}^{00})$ is given by $\widehat{\mathbf{K}}_h^{2h}(\boldsymbol{\theta}) = \widehat{\mathbf{I}}_h - \widehat{\mathbf{P}}_{2h}^h(\boldsymbol{\theta})(\widehat{\mathbf{L}}_{2h}(\boldsymbol{\theta}))^{-1}\widehat{\mathbf{R}}_h^{2h}(\boldsymbol{\theta})\widehat{\mathbf{L}}_h(\boldsymbol{\theta}) \in \mathbb{C}^{8\times 8}$, being $\widehat{\mathbf{I}}_h$, $\widehat{\mathbf{L}}_{2h}(\boldsymbol{\theta})$, $\widehat{\mathbf{L}}_h(\boldsymbol{\theta})$, $\widehat{\mathbf{R}}_h^{2h}(\boldsymbol{\theta})$ and $\widehat{\mathbf{P}}_{2h}^h(\boldsymbol{\theta})$ the Fourier representations in $\mathcal{F}^4(\boldsymbol{\theta}^{00})$ of the operators involved in the coarse grid correction. As a consequence, the spectral radius $\rho(M_h^{2h})$ can be calculated by means of the spectral radius of (8×8)–matrices, so it is possible to determine the asymptotic two–grid convergence factor as:

$$\rho_{2grid} = \rho(\mathbf{M}_h^{2h}) = \max_{\boldsymbol{\theta}^{00} \in \tilde{\boldsymbol{\Theta}}_{2h}} \rho(\widehat{\mathbf{M}}_h^{2h}(\boldsymbol{\theta}^{00})). \tag{5}$$

However, this is not true for three–color smoother, which leads us to consider another subdivision of the Fourier space to be explained next.

2.3.1 Two–grid analysis for three–color smoother

In the case of three–color smoother, the following decomposition of the Fourier space is considered $\mathcal{F}(G_h) = \oplus\mathcal{F}^{12}(\boldsymbol{\theta}_{00})$, where $\mathcal{F}^{12}(\boldsymbol{\theta}_{00}) = \mathcal{F}^3(\boldsymbol{\theta}_{00}^{00}) \oplus \mathcal{F}^3(\boldsymbol{\theta}_{00}^{11}) \oplus \mathcal{F}^3(\boldsymbol{\theta}_{00}^{10}) \oplus \mathcal{F}^3(\boldsymbol{\theta}_{00}^{01})$, where

$$\boldsymbol{\theta}_{00}^{00} = \boldsymbol{\theta}_{00} \in \boldsymbol{\Lambda}^{12} = \left(\left(-\frac{\pi}{3h_1}, \frac{\pi}{3h_1}\right] \times \left(-\frac{\pi}{3h_2}, \frac{\pi}{3h_2}\right]\right) \setminus \left(\left(0, \frac{\pi}{3h_1}\right] \times \left(0, \frac{\pi}{3h_2}\right]\right),$$

$\boldsymbol{\theta}_{00}^{11}, \boldsymbol{\theta}_{00}^{10}, \boldsymbol{\theta}_{00}^{01}$ are the three frequencies associated with $\boldsymbol{\theta}_{00}^{00}$ by means of (4) and the subspace $\mathcal{F}^3(\boldsymbol{\theta}_{00}^{ij})$ is generated as in (2). In Figure 6, the location of the twelve different frequencies $\boldsymbol{\theta}_{\alpha\alpha}^{ij}$ and the L–shaped region $\boldsymbol{\Lambda}^{12}$ is displayed.

As has been shown previously, $\mathcal{F}^3(\boldsymbol{\theta}_{00}^{ij})$ are invariant under $\mathbf{S}_h^i(\omega)$, and the matrix representation of $\mathbf{S}_h^0(\omega)$ in this space is a (6×6)–matrix which has the following form

$$\widehat{\mathbf{A}}^{ij}(\boldsymbol{\theta}_{00}, \omega) = \frac{1}{3}\begin{pmatrix} \mathbf{A}_{00}^{ij}(\boldsymbol{\theta}_{00}^{ij}, \omega) & \mathbf{A}_{11}^{ij}(\boldsymbol{\theta}_{00}^{ij}, \omega) & \mathbf{A}_{22}^{ij}(\boldsymbol{\theta}_{00}^{ij}, \omega) \\ \mathbf{A}_{00}^{ij}(\boldsymbol{\theta}_{11}^{ij}, \omega) & \mathbf{A}_{11}^{ij}(\boldsymbol{\theta}_{11}^{ij}, \omega) & \mathbf{A}_{22}^{ij}(\boldsymbol{\theta}_{11}^{ij}, \omega) \\ \mathbf{A}_{00}^{ij}(\boldsymbol{\theta}_{22}^{ij}, \omega) & \mathbf{A}_{11}^{ij}(\boldsymbol{\theta}_{22}^{ij}, \omega) & \mathbf{A}_{22}^{ij}(\boldsymbol{\theta}_{22}^{ij}, \omega) \end{pmatrix}^t,$$

with

$$\mathbf{A}_{\alpha'\alpha'}^{ij}(\boldsymbol{\theta}_{\alpha\alpha}^{ij}, \omega) = \begin{cases} \boldsymbol{\lambda}_{\alpha\alpha}^{ij}(\omega) + 2\mathbf{I}, & \text{if } \alpha' = \alpha, \\ \boldsymbol{\lambda}_{\alpha\alpha}^{ij}(\omega) - \mathbf{I}, & \text{otherwise,} \end{cases} \qquad \text{where} \quad \boldsymbol{\lambda}_{\alpha\alpha}^{ij}(\omega) = \widetilde{\mathbf{I}}_h - \omega\widetilde{\mathbf{D}}_h^{-1}(\boldsymbol{\theta}_{\alpha\alpha}^{ij})\widetilde{\mathbf{L}}_h(\boldsymbol{\theta}_{\alpha\alpha}^{ij}).$$

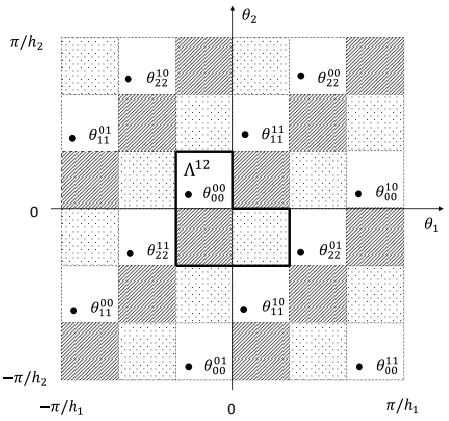

Figure 6: Twelve–dimensional minimal invariant harmonic subspaces.

For the partial smoothing operators $\mathbf{S}_h^1(\omega)$ and $\mathbf{S}_h^2(\omega)$ we have the matrices $\widehat{\mathbf{B}}^{ij}(\boldsymbol{\theta}_{00},\omega)$ and $\widehat{\mathbf{C}}^{ij}(\boldsymbol{\theta}_{00},\omega)$, whose coefficients are computed as in the case of the smoothing analysis. Consequently, $\mathcal{F}^{12}(\boldsymbol{\theta}_{00})$ are invariant for three–color smoother, and the matrix representation of $\mathbf{S}_h^i(\omega)$ and $\mathbf{S}_h(\omega)$ in this subspace are the following (24×24)–matrices:

$$\begin{aligned}
\widehat{\mathbf{S}}_h^0(\boldsymbol{\theta}_{00},\omega) &= \mathrm{diag}\{\widehat{\mathbf{A}}^{00}(\boldsymbol{\theta}_{00},\omega),\widehat{\mathbf{A}}^{11}(\boldsymbol{\theta}_{00},\omega),\widehat{\mathbf{A}}^{10}(\boldsymbol{\theta}_{00},\omega),\widehat{\mathbf{A}}^{01}(\boldsymbol{\theta}_{00},\omega)\},\\
\widehat{\mathbf{S}}_h^1(\boldsymbol{\theta}_{00},\omega) &= \mathrm{diag}\{\widehat{\mathbf{B}}^{00}(\boldsymbol{\theta}_{00},\omega),\widehat{\mathbf{B}}^{11}(\boldsymbol{\theta}_{00},\omega),\widehat{\mathbf{B}}^{10}(\boldsymbol{\theta}_{00},\omega),\widehat{\mathbf{B}}^{01}(\boldsymbol{\theta}_{00},\omega)\},\\
\widehat{\mathbf{S}}_h^2(\boldsymbol{\theta}_{00},\omega) &= \mathrm{diag}\{\widehat{\mathbf{C}}^{00}(\boldsymbol{\theta}_{00},\omega),\widehat{\mathbf{C}}^{11}(\boldsymbol{\theta}_{00},\omega),\widehat{\mathbf{C}}^{10}(\boldsymbol{\theta}_{00},\omega),\widehat{\mathbf{C}}^{01}(\boldsymbol{\theta}_{00},\omega)\},\\
\widehat{\mathbf{S}}_h(\boldsymbol{\theta}_{00},\omega) &= \widehat{\mathbf{S}}_h^2(\boldsymbol{\theta}_{00},\omega)\widehat{\mathbf{S}}_h^1(\boldsymbol{\theta}_{00},\omega)\widehat{\mathbf{S}}_h^0(\boldsymbol{\theta}_{00},\omega).
\end{aligned}$$

With regard to the coarse grid correction operator $\mathbf{K}_h^{2h}$, it leaves subspaces $\mathcal{F}^{12}(\boldsymbol{\theta}_{00})$ invariant. It turns out that the matrix representation of $\mathbf{K}_h^{2h}$ in this subspace is the following (24×24)–matrix:

$$\widehat{\mathbf{K}}_h^{2h}(\boldsymbol{\theta}_{00}) = \begin{pmatrix} \mathbf{K}_{11} & \mathbf{K}_{12} & \mathbf{K}_{13} & \mathbf{K}_{14}\\ \mathbf{K}_{21} & \mathbf{K}_{22} & \mathbf{K}_{23} & \mathbf{K}_{24}\\ \mathbf{K}_{31} & \mathbf{K}_{32} & \mathbf{K}_{33} & \mathbf{K}_{34}\\ \mathbf{K}_{41} & \mathbf{K}_{42} & \mathbf{K}_{43} & \mathbf{K}_{44} \end{pmatrix},$$

where $\mathbf{K}_{ij}$ is the block diagonal matrix $\mathbf{K}_{ij} = \mathrm{diag}\{\mathbf{c}_{0,ij},\mathbf{c}_{1,ij},\mathbf{c}_{2,ij}\}$, being $\mathbf{c}_{\alpha,ij}$ the (2×2)-block situated in the position (i,j) of matrix $\widehat{\mathbf{K}}_{\alpha,h}^{2h}(\boldsymbol{\theta}_{\alpha\alpha})$, which is built in the following way

$$\widehat{\mathbf{K}}_{\alpha,h}^{2h}(\boldsymbol{\theta}_{\alpha\alpha}) = \widehat{\mathbf{I}}_h - \widehat{\mathbf{P}}_{2h}^h(\boldsymbol{\theta}_{\alpha\alpha})(\widehat{\mathbf{L}}_{2h}(\boldsymbol{\theta}_{\alpha\alpha}))^{-1}\widehat{\mathbf{R}}_h^{2h}(\boldsymbol{\theta}_{\alpha\alpha})\widehat{\mathbf{L}}_h(\boldsymbol{\theta}_{\alpha\alpha}) \in \mathbb{C}^{8\times 8}.$$

In order to ensure that nonsingular Fourier symbols are taken, instead of $\boldsymbol{\Lambda}^{12}$ the following space is considered, $\widetilde{\boldsymbol{\Lambda}}^{12} = \boldsymbol{\Lambda}^{12}\setminus\{\boldsymbol{\theta}_{00}\in\boldsymbol{\Lambda}^{12}|\det(\widetilde{\mathbf{L}}_{2h}(2\boldsymbol{\theta}_{\alpha\alpha}^{00}))=0,\ \text{or}\ \det(\widetilde{\mathbf{L}}_h(\boldsymbol{\theta}_{\alpha\alpha}^{ij}))=0,\ i,j\in\{0,1\}\}$. And thus, the asymptotic convergence factor for ν_1 pre–smoothing and ν_2 post–smoothing steps of three–color smoother can be defined as

$$\rho_{2grid} = \rho(\mathbf{M}_h^{2h}) = \sup_{\boldsymbol{\theta}^{00}\in\tilde{\boldsymbol{\Lambda}}^{12}}\rho(\widehat{\mathbf{M}}_h^{2h}(\boldsymbol{\theta}^{00})) = \sup_{\boldsymbol{\theta}^{00}\in\tilde{\boldsymbol{\Lambda}}^{12}}\rho(\widehat{\mathbf{S}}_h^{\nu_1}(\boldsymbol{\theta}^{00},\omega)\widehat{\mathbf{K}}_h^{2h}(\boldsymbol{\theta}^{00})\widehat{\mathbf{S}}_h^{\nu_2}(\boldsymbol{\theta}^{00},\omega)).$$

3 Fourier analysis results

As is well-known, elasticity operator has the property of being invariant under Euclidean motions. Thus, if we consider a rotation by angle θ, elasticity operator $\mathbf{L}$ satisfies $\mathbf{L}(R\mathbf{u}) = R(\mathbf{L}\mathbf{u})$, where R is the rotation matrix given by

$$R = \begin{pmatrix} \cos\theta & -\sin\theta\\ \sin\theta & \cos\theta \end{pmatrix}.$$

As a consequence, it is easy to see that $\widetilde{\mathbf{L}}_{R,h} = R\,\widetilde{\mathbf{L}}_h R^t$, where $\widetilde{\mathbf{L}}_h$ and $\widetilde{\mathbf{L}}_{R,h}$ are the LFA symbols of the discrete operators associated with two grids, one obtained by rotating the other. Thus, it is fulfilled that these LFA symbols are similar and therefore LFA results obtained for these two grids are completely identical.
Due to this property it is possible to restrict the analysis to triangles that sit on the x-axis of the Cartesian coordinate system. Therefore, in this section Local Fourier Analysis is applied to a discretization of the elasticity operator by linear finite elements on a regular triangulation of a general triangle, in order to investigate how the grid–geometry has influence on the properties of multigrid methods.
This section focuses on analyzing different smoothers for the posed problem, while the components of the coarse–grid correction are taken as the standard ones as we have mentioned before. One of the proposals here is the three–color smoother. In order to support the choice of this smoother as a good option for some geometries, some results obtained comparing it with the point-wise Gauss-Seidel are presented. These results appear in Table 2, where their two–grid convergence factors ρ and also the experimentally measured W–cycle convergence factors, denoted by ρ_h and obtained with a zero right-hand side and a random initial guess, are shown in order to observe that convergence factors are very well predicted by LFA. These factors are computed for an equilateral triangle, and it can be observed that three-color smoother provides the best convergence factors between the two smoothers.

	Gauss–Seidel		Three–color smoother	
ν_1, ν_2	ρ	ρ_h	ρ	ρ_h
$1, 0$	0.516	0.506	0.422	0.422
$1, 1$	0.257	0.255	0.173	0.172
$2, 1$	0.172	0.172	0.097	0.095
$2, 2$	0.113	0.113	0.073	0.072

Table 2: Two–grid convergence factors ρ and measured W–cycle convergence rates ρ_h for equilateral triangles.

However, the three–color smoother is not robust over all angles, that is, the highly satisfactory factors obtained for equilateral triangles worsen when one of the angles of the triangle is small. This behavior can be seen in Table 3, where smoothing and two-grid factors obtained with this smoother are shown for some representative triangles.

	Equilateral		Isosceles (75^o)		Isosceles (85^o)	
ν_1, ν_2	$\mu^{\nu_1+\nu_2}$	ρ	$\mu^{\nu_1+\nu_2}$	ρ	$\mu^{\nu_1+\nu_2}$	ρ
$1, 0$	0.503	0.422	0.811	0.814	0.976	0.977
$1, 1$	0.253	0.173	0.657	0.661	0.954	0.955
$2, 1$	0.127	0.097	0.533	0.536	0.932	0.934
$2, 2$	0.064	0.073	0.432	0.435	0.911	0.913

Table 3: LFA smoothing and two–grid factors for different triangles with three-color smoother.

To overcome this difficulty, three zebra-type smoothers, associated with the three vertices of the triangle, are proposed. These zebra–type smoothers are preferred to the lexicographic block–line Gauss–Seidel smoothers because, despite having the same computational cost, they are more suitable for parallel implementation and their two-grid convergence factors are better, as we can see in Table 4 for an isosceles triangle with common angle 85^o. Each of these zebra–type smoothers are highly efficient when the angle corresponding to the vertex of its color is sufficiently small. This is shown in Table 5, where smoothing and two-grid factors for some representative triangles are shown.

As a final remark, it is observed that, depending on the geometry of the triangles, it is possible

	Lexicographic line-wise smoother		Zebra–type smoother	
ν_1, ν_2	ρ	ρ_h	ρ	ρ_h
$1, 0$	0.333	0.331	0.143	0.142
$1, 1$	0.151	0.145	0.071	0.069
$2, 1$	0.094	0.094	0.047	0.046
$2, 2$	0.063	0.062	0.036	0.034

Table 4: LFA two–grid convergence factors and measured W–cycle convergence rates ρ_h for isosceles triangles with common angle 85^o.

	Equilateral		Isosceles (75^o)		Isosceles (85^o)	
ν_1, ν_2	$\mu^{\nu_1+\nu_2}$	ρ	$\mu^{\nu_1+\nu_2}$	ρ	$\mu^{\nu_1+\nu_2}$	ρ
$1, 0$	0.535	0.404	0.387	0.165	0.265	0.143
$1, 1$	0.226	0.164	0.096	0.072	0.053	0.071
$2, 1$	0.104	0.088	0.034	0.047	0.034	0.047
$2, 2$	0.049	0.067	0.025	0.035	0.025	0.036

Table 5: LFA smoothing and two–grid factors for equilateral and isosceles triangles with zebra–type smoother.

to improve the convergence factors of three-color and zebra-type smoothers by means of a relaxation parameter, whereas for the point-wise Gauss-Seidel and lexicographic line-wise smoothers there is no improvement. For instance, in the case of equilateral triangles the obtained convergence factor for three-color smoother is about 0.422, and it can enhance to 0.303 taking a damped parameter $\omega = 1.1$.

4 Conclusions

A Local Fourier Analysis for multigrid methods on triangular grids for the problem of planar elasticity has been presented. Analogously to the scalar case, the key point of this analysis is to introduce an expression of the Fourier transform in new coordinate systems, both in space and in frequency variables, associated to reciprocal bases. This analysis makes highly accurate predictions of the performance of a multigrid algorithm and as a consequence, also the choice of the adequate components of the method for a given problem. In this paper LFA has been applied to study the planar elasticity system, and with the help of this analysis a three-color smoother and some zebra-type smoothers are proposed to obtain an efficient multigrid algorithm to solve this problem.

References

[1] B. Bergen, T. Gradl, F. Hülsemann, U. Rüde. *A massively parallel multigrid method for finite elements.* Comput. Sci. Eng., 8 (2006), pp. 56–62.

[2] A. Brandt. *Multi-level adaptive solutions to boundary-value problems.* Math. Comput., 31 (1977), pp. 333–390.

[3] F.J. Gaspar, J.L. Gracia, F.J. Lisbona. *Fourier analysis for multigrid methods on triangular grids.* Preprint Seminario Matemático García de Galdeano, Universidad de Zaragoza, 2 (2008).

[4] U. Trottenberg, C.W. Oosterlee, A. Schüller. *Multigrid.* Academic Press, New York, 2001.

[5] R. Wienands, W. Joppich. *Practical Fourier analysis for multigrid methods.* Chapman and Hall/CRC Press, 2005.